17

Implementation of constitutive equations for single crystals in finite element codes

Jean-Michel Scherer[a,b] and Jacques Besson[b]

[a]Université Paris-Saclay, CEA, Service d'Etude des Matériaux Irradiés, Gif-sur-Yvette, France, [b]Centre des Matériaux, Mines ParisTech — PSL Research University, UMR CNRS 7633, Evry, France

Glossary

Orthonormal basis	$\mathcal{R} = \{\underline{e}_1, \underline{e}_2, \underline{e}_2\}$
Vector	$\underline{a} = a_i \underline{e}_i$
2nd-order tensor	$\underset{\sim}{A} = A_{ij} \underline{e}_i \otimes \underline{e}_j$
Transpose	$\underset{\sim}{A}^T = A_{ji} \underline{e}_i \otimes \underline{e}_j$
Inverse	$\underset{\sim}{A}^{-1} = A_{ij}^{-1} \underline{e}_i \otimes \underline{e}_j$
Transpose of the inverse	$\underset{\sim}{A}^{-T} = A_{ji}^{-1} \underline{e}_i \otimes \underline{e}_j$
Scalar product	$\underline{a} \cdot \underline{b} = \displaystyle\sum_{i=1}^{3} a_i b_i$
Double contraction	$\underset{\sim}{A} : \underset{\sim}{B} = \displaystyle\sum_{i=1}^{3}\sum_{j=1}^{3} A_{ij} B_{ij}$
Tensorial product	$\underline{a} \otimes \underline{b} = a_i b_j \underline{e}_i \otimes \underline{e}_j$
Tensorial product	$\underset{\sim}{A} \otimes \underset{\sim}{B} = A_{ij} B_{kl} \underline{e}_i \otimes \underline{e}_j \otimes \underline{e}_k \otimes \underline{e}_l$
Tensorial product	$\underset{\sim}{A} \overline{\otimes} \underset{\sim}{B} = A_{il} B_{jk} \underline{e}_i \otimes \underline{e}_j \otimes \underline{e}_k \otimes \underline{e}_l$
Tensorial product	$\underset{\sim}{A} \underline{\otimes} \underset{\sim}{B} = A_{ik} B_{jl} \underline{e}_i \otimes \underline{e}_j \otimes \underline{e}_k \otimes \underline{e}_l$
Identity tensor (2nd-order)	$\underset{\sim}{1} = \delta_{ij} \underline{e}_i \otimes \underline{e}_j$
Identity tensor (4th-order)	$\underset{\approx}{1} = \frac{1}{2}\left(\delta_{ik}\delta_{jl} + \delta_{il}\delta_{jk}\right) \underline{e}_i \otimes \underline{e}_j \otimes \underline{e}_k \otimes \underline{e}_l$

The objective of this chapter is to give a description of the most efficient algorithms for the numerical implementation of crystal plasticity models in finite element codes. Of course, this approach requires a large amount of equations, which are provided in great detail. The specific notations used are grouped in a special section at the end of the chapter.

17.1 General form for the constitutive equations

17.1.1 Variables describing constitutive equations

The eventual programming of material characteristics within a finite element code will ideally respect the physical and mathematical foundations in form. Proper representation naturally leads to a complete interface between the global code design and the local (material). Essentially, this representation entails defining the appropriate variables used to characterize a material behavior [452]. These variables are listed below:

Input variables v_{IN}. They are primary imposed problem variables over which the behavior is integrated. These variables are computed at the element level using the problem degrees of freedom. In standard mechanics, they usually correspond to strains (the measure will depend on the problem formulation).

Output variables v_{OUT}. These variables are the direct result of the time integration of the constitutive equations which are then used to compute the internal forces at the elementary level. In standard mechanics, they usually correspond to stresses (the measure will depend on the problem formulation).

Internal/Integrated variables v_{in}. These variables represent quantities used to describe the material state. They often are expressed as thermodynamic state variables [510,818]. These variables need to be time integrated.

Auxiliary variables v_{aux}. They encode interesting information which does not directly define the material state. They are functions of v_{in} but do not need to be time integrated.

External Parameters EP. These parameters are quantities which are user-defined (prescribed) for the calculation but which influence the behavior. They, e.g., correspond to temperature for a purely mechanical simulation.

Material coefficients CO. These coefficients are used to define the constitutive behavior. Simple examples are elastic moduli, yield stress, hardening modulus, etc. They can depend on other quantities so that

$$\text{CO} = \text{CO}\left(v_{\text{in}}, v_{\text{aux}}, \text{EP}\right). \tag{17.1}$$

The class of behavior is thus characterized by the in–out variable types $v_{\mathrm{IN}}/v_{\mathrm{OUT}}$. In "standard" mechanics they will correspond to small deformation strain tensor / Cauchy stress (ε/σ), Green–Lagrange strain / second Piola–Kirchhoff stress ($\mathbf{E}/\mathbf{S}$), deformation gradient / first Piola–Kirchhoff stress ($\mathbf{F}/\mathit{\Pi}$), Hencky's logarithmic strain / work conjugate stress [943] ($\mathbf{H} = \frac{1}{2} \log \left(\mathbf{F}^T . \mathbf{F} \right) / \mathbf{T}$), etc. One has

$$\rho \dot{\varepsilon} : \sigma = \rho_0 \dot{\varepsilon} : \tau = \rho_0 \dot{\mathbf{E}} : \mathbf{S} = \rho_0 \dot{\mathbf{F}} : \mathit{\Pi} = \rho_0 \dot{\mathbf{H}} : \mathbf{T}, \qquad (17.2)$$

where τ is the Kirchhoff stress tensor and $\rho/\rho_0 = \det \mathbf{F}$.

When using implicit simulation codes, it is also required to compute the "consistent" tangent matrix which can be formally expressed as

$$[K] = \frac{d\Delta v_{\mathrm{OUT}}}{d\Delta v_{\mathrm{IN}}}, \qquad (17.3)$$

where Δv_{OUT} and Δv_{IN} represent the increments of output/input variables over a finite time increment Δt. In "standard" mechanics, $[K]$ corresponds to a fourth-order tensor.

17.1.2 Integration methods

17.1.2.1 *Explicit integration*

The evolution of integrated variables v_{in} is usually expressed as a set of differential equations

$$\dot{v}_{\mathrm{in}} = \mathcal{V}(v_{\mathrm{in}}, t, \mathrm{EP}, \mathrm{CO}, v_{\mathrm{aux}}). \qquad (17.4)$$

When considering this equation, one must indeed take into account that EP, depends on time, CO on v_{in}, EP, and v_{aux}, and v_{aux} on v_{in}. This can lead to some complex formulation, and it is important to keep track of the dependencies. Eq. (17.4) can therefore be rewritten in a more simple form as

$$\dot{v}_{\mathrm{in}} = \mathcal{V}(v_{\mathrm{in}}, t). \qquad (17.5)$$

Eq. (17.5) can be integrated using well-known numerical techniques. Describing these methods is indeed out of the scope of this text. Efficient methods such as the Runge–Kutta methods are, for instance, described in [180], and efficient implementations are now available. The main drawback of this method is that it does not provide a "consistent" tangent matrix $[K]$ so that specific developments are necessary to compute it. Note that a perturbation method can be used, but this tends to be very time-consuming as many integrations must be performed, possibly inaccurate and strongly dependent on the selected perturbation.

17.1.2.2 Implicit integration

Eq. (17.5) can be time integrated as

$$\Delta v_{\text{in}} = \mathcal{V}(v_{\text{in}}^{\theta}, t^{\theta})\Delta t, \tag{17.6}$$

where Δt is the time step and θ is a parameter such that $0 \leq \theta \leq 1$. The notation x^{θ} refers to the value of x at time $t^0 + \theta \Delta t$ where t^0 is the time at the beginning of the time step (so that x^0 is the value of x at the beginning of the time step and $x^{\theta} = x^0 + \theta \Delta x$). For $\theta = 0$, Eq. (17.6) corresponds to the simple forward Euler integration scheme which is known to be unstable. Stability is obtained provided $\theta > 1/2$. Eq. (17.6) is then rewritten as

$$\Delta v_{\text{in}} = \mathcal{V}(v_{\text{in}}^0 + \theta \Delta v_{\text{in}}, t^0 + \theta \Delta t)\Delta t, \tag{17.7}$$

so that it becomes obvious that this equation must be solved for the unknown value Δv_{in}. The equation can be reformulated as

$$R_{\text{in}} = \Delta v_{\text{in}} - \mathcal{V}(v_{\text{in}}^0 + \theta \Delta v_{\text{in}}, t^0 + \theta \Delta t)\Delta t = 0, \tag{17.8}$$

where R_{in} is the residual vector. Time integrating equation (17.4) becomes equivalent to solving (17.8). This equation is usually highly nonlinear and must be solved using, for instance, an iterative Newton–Raphson scheme. This requires the evaluation of the Jacobian matrix $[J]$ associated to (17.8), which is formally expressed as

$$[J] = \frac{\partial R_{\text{in}}}{\partial \Delta v_{\text{in}}} = [1] - \Delta t \left.\frac{\partial R_{\text{in}}}{\partial v_{\text{in}}}\right|_{\theta} \cdot \frac{\partial v_{\text{in}}}{\partial \Delta v_{\text{in}}} = [1] - \theta \Delta t \left.\frac{\partial R_{\text{in}}}{\partial v_{\text{in}}}\right|_{\theta}. \tag{17.9}$$

The evaluation of $[J]$ can be complex (see examples below). A perturbation technique can be used, but will possibly suffer from the drawbacks that have already been outlined above.

17.1.3 Consistent tangent matrix

Using the evaluation of the Jacobian matrix $[J]$ it becomes possible to compute the consistent tangent matrix at a relatively low cost. Eq. (17.8) was solved for fixed values of the input variables v_{IN}. To evaluate the infinitesimal variation of the integrated variables $(\delta \Delta v_{\text{in}})$ caused by an infinitesimal variation of the input variables $(\delta \Delta v_{\text{IN}})$, one must express that the residual must remain equal to 0. So that

$$\delta R_{\text{in}} = \frac{\partial R_{\text{in}}}{\partial \Delta v_{\text{in}}} \cdot \delta \Delta v_{\text{in}} + \frac{\partial R_{\text{in}}}{\partial \Delta v_{\text{IN}}} \cdot \delta \Delta v_{\text{IN}} = [J]_s \cdot \delta \Delta v_{\text{in}} + [L]_s \cdot \delta \Delta v_{\text{IN}} = 0, \tag{17.10}$$

where the subscript s denotes that the quantities are evaluated for Δv_{in} solution of Eq. (17.8) for the prescribed Δv_{IN}. Note that $[J]$ is a square matrix

which can be inverted; $[L]$ is usually not square. For the above equation, the following stiffness matrix can be evaluated:

$$[K]_{\text{in}} = \frac{\partial \Delta v_{\text{in}}}{\partial \Delta v_{\text{IN}}} = -[J]_s^{-1} \cdot [L]_s . \tag{17.11}$$

The output variables v_{OUT} are, however, usually not a subset of v_{in}. They are rather expressed explicitly as functions of v_{in} and v_{IN} so that

$$\delta \Delta v_{\text{OUT}} = \frac{\partial \Delta v_{\text{OUT}}}{\partial \Delta v_{\text{IN}}} \cdot \delta \Delta v_{\text{IN}} + \frac{\partial \Delta v_{\text{OUT}}}{\partial \Delta v_{\text{in}}} \cdot \delta \Delta v_{\text{in}} \tag{17.12}$$

$$= \left(\frac{\partial \Delta v_{\text{OUT}}}{\partial \Delta v_{\text{IN}}} + \frac{\partial \Delta v_{\text{OUT}}}{\partial \Delta v_{\text{in}}} \cdot [K]_{\text{in}} \right) \cdot \delta \Delta v_{\text{IN}}, \tag{17.13}$$

which leads to the final expression of the consistent stiffness matrix, namely

$$[K] = \frac{d \Delta v_{\text{OUT}}}{d \Delta v_{\text{IN}}} = \frac{\partial \Delta v_{\text{OUT}}}{\partial \Delta v_{\text{IN}}} + \frac{\partial \Delta v_{\text{OUT}}}{\partial \Delta v_{\text{in}}} \cdot [K]_{\text{in}} . \tag{17.14}$$

Examples of these derivations will be given below in the case of the implementation of the constitutive equations for single crystals.

17.2 A small strain constitutive model for single crystals

In the realm of elasto-plasticity of single crystals, it is commonly admitted that elastic deformations are related to the stretching of interatomic bonds, while plastic deformations are due to the gliding of linear defects in the crystal lattice called dislocations. Dislocation glide occurs preferentially on particular planes, which are denoted by unit normal $\underline{\mathbf{n}}^\alpha$, and in particular directions, oriented by unit vector $\underline{\mathbf{m}}^\alpha$. The type of slip systems (plane/direction) vary upon the kind of crystal lattice (body-centered cubic, face-centered cubic, hexagonal compact, etc.) considered. A convenient way to model plastic deformations in crystals consist in decomposing the overall plastic strain tensor into a sum of shear mechanisms over the slip systems. The motion of a dislocation induces indeed an irreversible shear strain. Locally, for each slip system, the amount of plastic shear strain can be quantified by a scalar value noted γ^α. In addition, in order to represent the population of dislocations in the crystal, a scalar dislocation density per slip system ρ^α is defined. It corresponds to the length of dislocation line per unit volume for a given systems and thus has a unit of m/m^3, i.e., m^{-2}. Since dislocation densities are for most crystals in the range 10^6–10^{16} m^{-2}, it is numerically more convenient to manipulate dimensionless dislocation densities defined as $r^\alpha = \epsilon b^2 \rho^\alpha$. The scalar b denotes the norm of the Burgers vector, while ϵ is a nonphysical parameter

used in order to scale dimensionless dislocation densities to numerical values that are close to the typical order of magnitudes encountered for strain measures. Typically, $\epsilon = 10^6$ can be used. Within a small strain framework, such a model for the elasto-plasticity of single crystals yields the following sets of input, output, and internal variables:

$$v_{\text{IN}} : \{\underset{\sim}{\varepsilon}\}, \quad v_{\text{OUT}} : \{\underset{\sim}{\sigma}\}, \quad v_{\text{in}} : \{\underset{\sim}{\varepsilon}^e, \gamma^\alpha, r^\alpha\}, \tag{17.15}$$

where $\underset{\sim}{\varepsilon}^e$ denotes the elastic strain tensor. Any increment of the elastic strain tensor is linearly related to an increment of the Cauchy stress tensor $\underset{\sim}{\sigma}$,

$$\Delta\underset{\sim}{\sigma} = \underset{\approx}{\mathbf{C}} : \Delta\underset{\sim}{\varepsilon}^e, \tag{17.16}$$

where $\underset{\approx}{\mathbf{C}}$ denotes the fourth-order elasticity tensor. From a numerical point of view, it means that computing the unique output variable is a mere postprocessing of one of the integration procedure result, namely $\Delta\underset{\sim}{\varepsilon}^e$. As discussed earlier, plastic deformation in crystals is accounted for by a set of shear mechanisms acting on several slip systems. The driving force on a given slip plane in a given slip direction is called the resolved shear stress τ^α and is related to the symmetric Schmid tensor $\underset{\sim}{\mathbf{N}}_s^\alpha$ as follows:

$$\tau^\alpha = \underset{\sim}{\sigma} : \underset{\sim}{\mathbf{N}}_s^\alpha, \qquad \underset{\sim}{\mathbf{N}}_s^\alpha = \frac{1}{2}(\underline{\mathbf{m}}^\alpha \otimes \underline{\mathbf{n}}^\alpha + \underline{\mathbf{n}}^\alpha \otimes \underline{\mathbf{m}}^\alpha). \tag{17.17}$$

Within the small-strain setting considered in this section, an additive split of the strain tensor increment into elastic and plastic parts can be assumed. In light of the plastic deformation mode described above, the plastic increment can in turn be decomposed into a sum of shear modes increments over each slip system. It comes to

$$\Delta\underset{\sim}{\varepsilon} = \Delta\underset{\sim}{\varepsilon}^e + \Delta\underset{\sim}{\varepsilon}^p = \Delta\underset{\sim}{\varepsilon}^e + \sum_{\alpha=1}^{N} \frac{\Delta\gamma^\alpha}{2}(\underline{\mathbf{m}}^\alpha \otimes \underline{\mathbf{n}}^\alpha + \underline{\mathbf{n}}^\alpha \otimes \underline{\mathbf{m}}^\alpha), \tag{17.18}$$

where N denotes the total number of slip systems. Now, the amount of plastic slip increment over each slip system relies on mainly two aspects. First of all, it depends upon the resistance to dislocation glide, i.e., the stress barrier to overcome in order to put dislocations into motion. Such a barrier is called the critical resolved shear stress τ_c^α. Following [463], a form of the critical resolved shear is assumed as

$$\tau_c^\alpha = \tau_0^\alpha + \alpha\mu \sqrt{\sum_{\beta=1}^{N} a^{\alpha\beta} r^\beta}, \tag{17.19}$$

where the first term τ_0^α is a material parameter that varies upon temperature. The second term models the hardening related to forest dislocations.

Dislocation motion in a given slip system can indeed be hindered by dislocations lying in the same or others systems. Such impediments depend upon the nature of the junction or dipoles that two dislocations can form and are characterized by the magnitude of the coefficients involved in the interaction matrix a^{su}. The second aspects on which relies the amount of plastic increment on a given slip system is the resolved shear stress τ^α acting on its slip plane and in its direction of dislocation glide; τ^α needs to be large enough in order to overcome the aforementioned barrier τ_c^α. In other words, the yield locus for a given slip system follows Schmid's law and is given by

$$f^\alpha = |\tau^\alpha| - \tau_c^\alpha. \tag{17.20}$$

Because of the symmetries existing in crystal lattices, slip systems are mostly not unique and hence crystal plasticity inherits a multisurface yield domain by construction. It is well known that such a surface can have sharp edges and even corners. Therefore, if one assumes an associated flow rule, such that the plastic strain rate develops perpendicularly to the yield locus, indeterminacy of the plastic strain rate arises at edges and corners since the normal is not uniquely defined. In rate-independent crystal plasticity, the ill-posed problem of determining the set of active slip systems and associated slip rates was addressed in various manner. Numerical methods involving generalized or pseudoinverses [944,1624], or augmented Lagrangian formulations [1279] were proposed. Alternatively, [458] developed a rate-independent formulation of crystal plasticity based on a smooth elastic-plastic transition which involves a rate-independent overstress. Another possible alternative to overcome slip indeterminacy commonly encountered in the literature consists in smoothing out corners and edges by using viscoplastic flow rules in order to determine active systems and slip rates [174]. The latter option is adopted in what follows. Using a Norton-type viscous flow rule, the plastic slip increment is therefore written as

$$\Delta\gamma^\alpha = \text{sign}\left(\tau^\alpha\right)\Delta t\,\dot{\gamma}_0\Phi(f^\alpha), \qquad \Phi(f^\alpha) = \left\langle \frac{f^\alpha}{\tau_0^\alpha} \right\rangle^n, \tag{17.21}$$

where $\dot{\gamma}_0$ and n are viscosity material parameters. The induced viscous overstress is indeed equal to $\tau_0^\alpha(\Delta\gamma^\alpha/(\Delta t\dot{\gamma}_0))^{1/n} = \tau_0^\alpha(\dot{\gamma}^\alpha/\dot{\gamma}_0)^{1/n}$. Using large values for both parameters allows pushing such a rate-dependent model towards a quasi-rate-independent limit. However, from a numerical point of view, increasing these parameters without precaution renders the set of differential equations overly stiff and prevents from the possibility of using large time steps. Finally, in order to close the system of equations, evolution equations for the dislocation densities r^α need to be defined. These evolutionary laws are based on two main phenomena, namely storage and recovery of dislocations [1407,734]. Storage occurs

by pinning of dislocations after they have glided over a certain mean free path, controlled by the dimensionless material parameter κ. Recovery takes place by annihilation of screw dislocations thanks to cross-slip. The dimensionless material parameter G_c characterizes the distance at which annihilation can occur. The increment of dislocation density is related to the plastic slip increment on the same slip system and dislocation densities on all slip systems as follows:

$$\Delta r^\alpha = |\Delta\gamma^\alpha| \left(\frac{1}{\kappa} \sqrt{\sum_{\beta=1}^{N} b^{\alpha\beta} r^\beta} - G_c r^\alpha \right), \tag{17.22}$$

where b^{sr} denotes another interaction matrix characterizing dislocation storage.

Over a time increment, we recall that the unknowns to be determined are the increments of integrated variables, namely $\Delta\underset{\sim}{\varepsilon}^e$, $\Delta\gamma^\alpha$, and Δr^α. The set of nonlinear differential equations defined in Eqs. (17.18), (17.21), and (17.22) can be recast in a set of residuals R_{in} as follows:

$$R_{\text{in}} = \begin{cases} R_{\underset{\sim}{\varepsilon}^e} & = \Delta\underset{\sim}{\varepsilon}^e + \Delta\underset{\sim}{\varepsilon}^p - \Delta\underset{\sim}{\varepsilon}, \\[2mm] R_{\gamma^\alpha} & = \Delta\gamma^\alpha - \text{sign}\,(\tau^\alpha)\,\Delta t\dot{\gamma}_0\Phi(f^\alpha), \\[2mm] R_{r^\alpha} & = \Delta r^\alpha - |\Delta\gamma^\alpha| \left(\frac{1}{\kappa} \sqrt{\sum_{\beta=1}^{N} b^{\alpha\beta} r^\beta} - G_c r^\alpha \right). \end{cases} \tag{17.23}$$

In order to solve $R_{\text{in}} = 0$ by Newton's method, the Jacobian matrix of Eq. (17.23) can be calculated as follows:

$$[J] = \frac{\partial R_{\text{in}}}{\partial \Delta v_{\text{in}}} = \begin{pmatrix} \dfrac{\partial R_{\underset{\sim}{\varepsilon}^e}}{\partial \Delta\underset{\sim}{\varepsilon}^e} & \dfrac{\partial R_{\underset{\sim}{\varepsilon}^e}}{\partial \Delta\gamma^\beta} & \dfrac{\partial R_{\underset{\sim}{\varepsilon}^e}}{\partial \Delta r^\beta} \\[4mm] \dfrac{\partial R_{\gamma^\alpha}}{\partial \Delta\underset{\sim}{\varepsilon}^e} & \dfrac{\partial R_{\gamma^\alpha}}{\partial \Delta\gamma^\beta} & \dfrac{\partial R_{\gamma^\alpha}}{\partial \Delta r^\beta} \\[4mm] \dfrac{\partial R_{r^\alpha}}{\partial \Delta\underset{\sim}{\varepsilon}^e} & \dfrac{\partial R_{r^\alpha}}{\partial \Delta\gamma^\beta} & \dfrac{\partial R_{r^\alpha}}{\partial \Delta r^\beta} \end{pmatrix}, \tag{17.24}$$

- $R_{\underset{\sim}{\varepsilon}^e}$

$$R_{\underset{\sim}{\varepsilon}^e} = \Delta\underset{\sim}{\varepsilon}^e + \Delta\underset{\sim}{\varepsilon}^p - \Delta\underset{\sim}{\varepsilon}, \tag{17.25}$$

$$\frac{\partial R_{\underset{\sim}{\varepsilon}^e}}{\partial \Delta\underset{\sim}{\varepsilon}^e} = \mathbf{1}, \qquad \frac{\partial R_{\underset{\sim}{\varepsilon}^e}}{\partial \Delta\gamma^\beta} = \mathbf{N}_s^\beta, \qquad \frac{\partial R_{\underset{\sim}{\varepsilon}^e}}{\partial \Delta r^\beta} = 0; \tag{17.26}$$

- R_{γ^α}

$$R_{\gamma^\alpha} = \Delta\gamma^\alpha - \text{sign}\,(\tau^\alpha)\,\Delta t\dot{\gamma}_0\Phi(f^\alpha), \tag{17.27}$$

$$\frac{\partial R_{\gamma^\alpha}}{\partial \Delta \underset{\sim}{\varepsilon}^e} = -\text{sign}\left(\tau^\alpha\right) \Delta t \dot{\gamma}_0 \frac{\partial \Phi^\alpha}{\partial f^\alpha} \frac{\partial f^\alpha}{\partial \tau^\alpha} \frac{\partial \tau^\alpha}{\partial \underset{\sim}{\sigma}} : \frac{\partial \underset{\sim}{\sigma}}{\partial \Delta \underset{\sim}{\varepsilon}^e} \tag{17.28}$$

$$= -\frac{\Delta t \dot{\gamma}_0 n}{(\tau_0^\alpha)^n} \left\langle \frac{f^\alpha}{\tau_0^\alpha} \right\rangle^{n-1} \underset{\sim}{\mathbf{N}}_s^\alpha : \underset{\sim}{\mathbf{C}}, \tag{17.29}$$

$$\frac{\partial R_{\gamma^\alpha}}{\partial \Delta \gamma^\beta} = \delta_{\alpha\beta}, \tag{17.30}$$

$$\frac{\partial R_{\gamma^\alpha}}{\partial \Delta r^\beta} = -\text{sign}\left(\tau^\alpha\right) \Delta t \dot{\gamma}_0 \frac{\partial \Phi^\alpha}{\partial f^\alpha} \frac{\partial f^\alpha}{\partial \tau_c^\alpha} \frac{\partial \tau_c^\alpha}{\partial \Delta r^\beta} \tag{17.31}$$

$$= \text{sign}\left(\tau^\alpha\right) \frac{\Delta t \dot{\gamma}_0 n}{(\tau_0^\alpha)^n} \left\langle \frac{f^\alpha}{\tau_0^\alpha} \right\rangle^{n-1} \frac{\alpha \mu a^{\alpha\beta}}{2} \left(\sum_{u=1}^N a^{\alpha u} r^u \right)^{-\frac{1}{2}}; \tag{17.32}$$

- R_{r^α}

$$R_{r^\alpha} = \Delta r^\alpha - |\Delta \gamma^\alpha| \left(\frac{1}{\kappa} \sqrt{\sum_{\beta=1}^N b^{\alpha\beta} r^\beta} - G_c r^\alpha \right), \tag{17.33}$$

$$\frac{\partial R_{r^\alpha}}{\partial \Delta \underset{\sim}{\varepsilon}^e} = 0, \tag{17.34}$$

$$\frac{\partial R_{r^\alpha}}{\partial \Delta \gamma^\beta} = -\text{sign}\left(\Delta \gamma^\alpha\right) \delta_{\alpha\beta} \left(\frac{1}{\kappa} \sqrt{\sum_{u=1}^N b^{\alpha u} r^u} - G_c r^\alpha \right), \tag{17.35}$$

$$\frac{\partial R_{r^\alpha}}{\partial \Delta r^\beta} = \delta_{\alpha\beta} - |\Delta \gamma^\alpha| \left(\frac{b^{\alpha\beta}}{2\kappa} \left(\sum_{u=1}^N b^{\alpha u} r^u \right)^{-\frac{1}{2}} - G_c \delta_{\alpha\beta} \right). \tag{17.36}$$

Following Eq. (17.14), the consistent tangent matrix can finally be computed. As $v_{\text{OUT}} = \underset{\sim}{\sigma}$, $v_{\text{IN}} = \underset{\sim}{\varepsilon}$, and $\underset{\sim}{\sigma} = \underset{\sim}{\mathbf{C}} : \underset{\sim}{\varepsilon}_e$, one has with block-matrix notations:

$$\frac{\partial \Delta v_{\text{OUT}}}{\partial \Delta v_{\text{IN}}} = 0, \qquad \frac{\partial \Delta v_{\text{OUT}}}{\partial \Delta v_{\text{in}}} = \left(\begin{array}{c|c} \underset{\sim}{\mathbf{C}} & [0] \end{array} \right), \qquad [L]_s = \frac{\partial R_{\text{in}}}{\partial \Delta v_{\text{IN}}} = \left(\begin{array}{c} -\underset{\sim}{\mathbf{1}} \\ \hline [0] \end{array} \right), \tag{17.37}$$

which leads to

$$[K] = \frac{d \Delta v_{\text{OUT}}}{d \Delta v_{\text{IN}}} = \frac{d \Delta \underset{\sim}{\sigma}}{d \Delta \underset{\sim}{\varepsilon}} = -\left(\begin{array}{c|c} \underset{\sim}{\mathbf{C}} & [0] \end{array} \right) . [J]_s^{-1} . \left(\begin{array}{c} -\underset{\sim}{\mathbf{1}} \\ \hline [0] \end{array} \right) \tag{17.38}$$

$$= \left(\begin{array}{c|c} \underset{\sim}{\mathbf{C}} & [0] \end{array} \right) . [J]_s^{-1} . \left(\begin{array}{c} \underset{\sim}{\mathbf{1}} \\ \hline [0] \end{array} \right), \tag{17.39}$$

where $[J]_s^{-1}$ can be expressed as a block matrix

$$[J]_s^{-1} = \left(\begin{array}{c|c} \underset{\sim}{\mathbf{L}}_e & [\ldots] \\ \hline [\ldots] & [\ldots] \end{array} \right) \tag{17.40}$$

so that the consistent tangent matrix can be more simply expressed as a product of fourth-order tensors

$$[K] = \underset{\approx}{\mathbf{C}} : \underset{\approx}{\mathbf{L}}_e. \tag{17.41}$$

17.3 A finite-strain constitutive model for single crystals

The constitutive model of elasto-plasticity in single crystals presented at small strains in the previous section is extended to finite strains in this section. The physical foundations are essentially unchanged and, as a consequence, attention is drawn to the numerical implications of the chosen finite-strain framework. The latter is based on the multiplicative decomposition of the deformation gradient $\underset{\sim}{\mathbf{F}}$ into an elastic part $\underset{\sim}{\mathbf{E}}$ and a plastic part $\mathbf{P}$ [814,901]. The sets of input, output, and internal variables are respectively chosen as

$$v_{\text{IN}} : \{\underset{\sim}{\mathbf{F}}\}, \quad v_{\text{OUT}} : \{\underset{\sim}{\mathit{\Pi}}\}, \quad v_{\text{int}} : \{\underset{\sim}{\mathbf{E}}, \gamma^\alpha, r^\alpha\}. \tag{17.42}$$

Compared to previous section, $\underset{\sim}{\varepsilon}$ is replaced by $\underset{\sim}{\mathbf{F}}$, and accordingly its work-conjugate $\underset{\sim}{\sigma}$ is replaced by the first Piola–Kirchhoff stress $\underset{\sim}{\mathit{\Pi}}$. It is recalled that $\underset{\sim}{\mathit{\Pi}}$ is connected to the Cauchy stress tensor through

$$\underset{\sim}{\mathit{\Pi}} = \det \underset{\sim}{\mathbf{F}} \underset{\sim}{\sigma} \cdot \underset{\sim}{\mathbf{F}}^{-T}. \tag{17.43}$$

The elastic small strain tensor $\underset{\sim}{\varepsilon}^e$ is replaced by $\underset{\sim}{\mathbf{E}}$. It can already be noted that the stress and strain measures considered in this formulation are no longer necessarily symmetric. According to the multiplicative decomposition of $\underset{\sim}{\mathbf{F}}$, elastic and plastic velocity gradients $\underset{\sim}{\mathbf{L}}^e$ and $\underset{\sim}{\mathbf{L}}^p$ can be introduced as follows:

$$\underset{\sim}{\mathbf{F}} = \underset{\sim}{\mathbf{E}} \cdot \underset{\sim}{\mathbf{P}}, \qquad \underset{\sim}{\mathbf{L}} = \dot{\underset{\sim}{\mathbf{F}}} \cdot \underset{\sim}{\mathbf{F}}^{-1} = \underset{\sim}{\mathbf{L}}^e + \underset{\sim}{\mathbf{E}} \cdot \underset{\sim}{\mathbf{L}}^p \cdot \underset{\sim}{\mathbf{E}}^{-1}, \tag{17.44}$$

$$\underset{\sim}{\mathbf{L}}^e = \dot{\underset{\sim}{\mathbf{E}}} \cdot \underset{\sim}{\mathbf{E}}^{-1}, \qquad \underset{\sim}{\mathbf{L}}^p = \dot{\underset{\sim}{\mathbf{P}}} \cdot \underset{\sim}{\mathbf{P}}^{-1} = \sum_{\alpha=1}^{N} \dot{\gamma}^\alpha \underline{\mathbf{m}}^\alpha \otimes \underline{\mathbf{n}}^\alpha. \tag{17.45}$$

The velocity gradient split is to be put in parallel with its small-strain counterpart in Eq. (17.18). The major difference here is the asymmetric character

of the plastic velocity gradient. At this point, the thermodynamical backbone of the present model, that is eluded for conciseness, motivates introducing the elastic Green–Lagrange strain measure $\underset{\sim}{\mathbf{E}}^e_{GL}$, the elastic second Piola–Kirchhoff stress measure $\underset{\sim}{\mathit{\Pi}}^e$, and the Mandel stress measure $\underset{\sim}{\mathit{\Pi}}^M$ as

$$\underset{\sim}{\mathbf{E}}^e_{GL} = \frac{1}{2}\left(\underset{\sim}{\mathbf{E}}^T \cdot \underset{\sim}{\mathbf{E}} - \underset{\sim}{\mathbf{1}}\right), \tag{17.46}$$

$$J = \det \underset{\sim}{\mathbf{F}} = \det \underset{\sim}{\mathbf{E}} \cdot \underset{\sim}{\mathbf{P}} = \det \underset{\sim}{\mathbf{E}} \det \underset{\sim}{\mathbf{P}} = J_e J_p, \tag{17.47}$$

$$\underset{\sim}{\mathit{\Pi}}^e = J_e \underset{\sim}{\mathbf{E}}^{-1} \cdot \underset{\sim}{\sigma} \cdot \underset{\sim}{\mathbf{E}}^{-T} = J_p^{-1} \underset{\sim}{\mathbf{E}}^{-1} \cdot \underset{\sim}{\mathbf{S}} \cdot \underset{\sim}{\mathbf{P}}^T, \tag{17.48}$$

$$\underset{\sim}{\mathit{\Pi}}^M = \underset{\sim}{\mathbf{E}}^T \cdot \underset{\sim}{\mathbf{E}} \cdot \underset{\sim}{\mathit{\Pi}}^e. \tag{17.49}$$

The state law equation (17.16) is replaced at finite strains by

$$\Delta \underset{\sim}{\mathit{\Pi}}^e = \underset{\approx}{\mathbf{C}} : \Delta \underset{\sim}{\mathbf{E}}^e_{GL}, \tag{17.50}$$

while $\underset{\sim}{\mathit{\Pi}}^e$ is power-conjugate to the elastic Green–Lagrange strain rate and $\underset{\sim}{\mathit{\Pi}}^M$ is power-conjugate to the plastic velocity gradient $\dot{\underset{\sim}{\mathbf{P}}} \cdot \mathbf{P}^{-1}$. Therefore the driving forces for plastic slip activity, namely the resolved shear stresses τ^α, are defined as follows:

$$\tau^\alpha = \underset{\sim}{\mathit{\Pi}}^M : \mathbf{N}^\alpha, \qquad \mathbf{N}^\alpha = \underline{\mathbf{m}}^\alpha \otimes \underline{\mathbf{n}}^\alpha, \tag{17.51}$$

where $\mathbf{N}^\alpha$ corresponds to the asymmetric Schmid tensor. It is worth noting that, although the definitions of resolved shear stresses are slightly generalized in Eq. (17.51) compared to (17.17), the formalism setup for crystal plasticity at small strains remains valid at finite strains. In other words, Eqs. (17.19), (17.20), (17.21), and (17.22) stay unchanged. From Eqs. (17.44) and (17.45), and straightforward algebraic manipulations, one obtains the only formally modified residual equation, namely that related to the incremental elastic-plastic split,

$$R_{\underset{\sim}{\mathbf{E}}} = \Delta \underset{\sim}{\mathbf{E}} - \Delta \underset{\sim}{\mathbf{F}} \cdot \underset{\sim}{\mathbf{F}}^{-1} \cdot \underset{\sim}{\mathbf{E}} - \underset{\sim}{\mathbf{E}} \cdot \left(\sum_{\alpha=1}^N \Delta \gamma^\alpha \underset{\sim}{\mathbf{N}}^\alpha\right) = 0. \tag{17.52}$$

Since only the first residual equation is formally modified in Eq. (17.23), only the terms in the first row and first column of the Jacobian matrix $[J]$ are affected:

$$[J] = \frac{\partial R_{\text{in}}}{\partial \Delta v_{\text{in}}} = \begin{pmatrix} \dfrac{\partial R_{\underset{\sim}{\mathbf{E}}}}{\partial \Delta \underset{\sim}{\mathbf{E}}} & \dfrac{\partial R_{\underset{\sim}{\mathbf{E}}}}{\partial \Delta \gamma^\beta} & \dfrac{\partial R_{\underset{\sim}{\mathbf{E}}}}{\partial \Delta r^\beta} \\[2ex] \dfrac{\partial R_{\gamma^\alpha}}{\partial \Delta \underset{\sim}{\mathbf{E}}} & \dfrac{\partial R_{\gamma^\alpha}}{\partial \Delta \gamma^\beta} & \dfrac{\partial R_{\gamma^\alpha}}{\partial \Delta r^\beta} \\[2ex] \dfrac{\partial R_{r^\alpha}}{\partial \Delta \underset{\sim}{\mathbf{E}}} & \dfrac{\partial R_{r^\alpha}}{\partial \Delta \gamma^\beta} & \dfrac{\partial R_{r^\alpha}}{\partial \Delta r^\beta} \end{pmatrix}, \tag{17.53}$$

- $R_{\underset{\sim}{E}}$

$$R_{\underset{\sim}{E}} = \Delta\underset{\sim}{E} - \Delta\underset{\sim}{F} \cdot \underset{\sim}{F}^{-1} \cdot \underset{\sim}{E} + \underset{\sim}{E} \cdot \left(\sum_{\alpha=1}^{N} \Delta\gamma^{\alpha} \underset{\sim}{N}^{\alpha} \right), \tag{17.54}$$

$$\frac{\partial R_{\underset{\sim}{E}}}{\partial \Delta\underset{\sim}{E}} = \underset{\sim}{1} - (\Delta\underset{\sim}{F} \cdot \underset{\sim}{F}^{-1})\underline{\otimes}\underset{\sim}{1} + \underset{\sim}{1}\underline{\otimes}\left(\sum_{\alpha=1}^{N} \Delta\gamma^{\alpha} \underset{\sim}{N}^{\alpha} \right)^{T}, \tag{17.55}$$

$$\frac{\partial R_{\underset{\sim}{E}}}{\partial \Delta\gamma^{\beta}} = \underset{\sim}{E} \cdot \underset{\sim}{N}^{\beta}, \qquad \frac{\partial R_{\underset{\sim}{E}}}{\partial \Delta r^{\beta}} = 0; \tag{17.56}$$

- $R_{\gamma^{\alpha}}$

$$R_{\gamma^{\alpha}} = \Delta\gamma^{\alpha} - \text{sign}\left(\tau^{\alpha}\right) \Delta t \dot{\gamma}_0 \Phi(f^{\alpha}), \tag{17.57}$$

$$\frac{\partial R_{\gamma^{\alpha}}}{\partial \Delta\underset{\sim}{E}} = -\text{sign}\left(\tau^{\alpha}\right) \Delta t \dot{\gamma}_0 \frac{\partial \Phi^{\alpha}}{\partial f^{\alpha}} \frac{\partial f^{\alpha}}{\partial \tau^{\alpha}} \frac{\partial \tau^{\alpha}}{\partial \underset{\sim}{\Pi}^M} : \frac{\partial \underset{\sim}{\Pi}^M}{\partial \underset{\sim}{C}^e} : \frac{\partial \underset{\sim}{C}^e}{\partial \underset{\sim}{E}} : \frac{\partial \underset{\sim}{E}}{\partial \Delta\underset{\sim}{E}}, \tag{17.58}$$

$$\underset{\sim}{C}^e = \underset{\sim}{E}^T \cdot \underset{\sim}{E} \tag{17.59}$$

$$\frac{\partial \underset{\sim}{\Pi}^M}{\partial \underset{\sim}{C}^e} = \frac{\partial \left[\underset{\sim}{C}^e \cdot \left(\underset{\approx}{C} : \frac{1}{2}(\underset{\sim}{C}^e - 1) \right) \right]}{\partial \underset{\sim}{C}^e} = (\underset{\sim}{1}\underline{\otimes}\underset{\sim}{\Pi}^{eT}) + \frac{1}{2}(\underset{\sim}{C}^e\underline{\otimes}\underset{\sim}{1}) : \underset{\approx}{C}, \tag{17.60}$$

$$\frac{\partial \underset{\sim}{C}^e}{\partial \underset{\sim}{E}} = \underset{\sim}{1}\overline{\otimes}\underset{\sim}{E}^T + \underset{\sim}{E}^T\underline{\otimes}\underset{\sim}{1}, \qquad \frac{\partial \underset{\sim}{E}}{\partial \Delta\underset{\sim}{E}} = \underset{\sim}{1}, \tag{17.61}$$

$$\frac{\partial R_{\gamma^{\alpha}}}{\partial \Delta\underset{\sim}{E}} = -\frac{\Delta t \dot{\gamma}_0 n}{(\tau_0^{\alpha})^n} \left\langle \frac{f^{\alpha}}{\tau_0^{\alpha}} \right\rangle^{n-1} \underset{\sim}{N}^s : \left(\underset{\sim}{1}\underline{\otimes}\underset{\sim}{\Pi}^e + \frac{1}{2}(\underset{\sim}{C}^e\underline{\otimes}\underset{\sim}{1}) : \underset{\approx}{C} \right) : (\underset{\sim}{1}\overline{\otimes}\underset{\sim}{E}^T + \underset{\sim}{E}^T\underline{\otimes}\underset{\sim}{1}); \tag{17.62}$$

- $R_{r^{\alpha}}$

$$R_{r^{\alpha}} = \Delta r^{\alpha} - |\Delta\gamma^{\alpha}| \left(\frac{1}{\kappa} \sqrt{\sum_{\beta=1}^{N} b^{\alpha\beta} r^{\beta}} - G_c r^{\alpha} \right), \tag{17.63}$$

$$\frac{\partial R_{r^{\alpha}}}{\partial \Delta\underset{\sim}{E}} = 0. \tag{17.64}$$

The derivatives which intervene in the consistent tangent matrix are then calculated as follows:

$$\frac{\partial \Delta v_{\text{OUT}}}{\partial \Delta v_{\text{IN}}} = \frac{\partial \Delta\underset{\sim}{\Pi}}{\partial \Delta\underset{\sim}{F}} = \frac{\partial \Delta \left(J\underset{\sim}{\sigma} \cdot \underset{\sim}{F}^{-T} \right)}{\partial \Delta\underset{\sim}{F}} \tag{17.65}$$

$$= J(\underset{\sim}{\sigma} \cdot \underset{\sim}{\mathbf{F}}^{-T}) \otimes \underset{\sim}{\mathbf{F}}^{-T} + J(\underset{\sim}{\sigma} \underline{\otimes} \mathbf{1}) : (-\underset{\sim}{\mathbf{F}}^{-T} \overline{\otimes} \underset{\sim}{\mathbf{F}}^{-1}), \tag{17.66}$$

$$\frac{\partial \Delta v_{\text{OUT}}}{\partial \Delta v_{\text{in}}} = \left(\left. \frac{\partial \Delta \underset{\sim}{\Pi}}{\partial \Delta \underset{\sim}{\mathbf{E}}} \right| [0] \right), \tag{17.67}$$

$$\frac{\partial \Delta \underset{\sim}{\Pi}}{\partial \Delta \underset{\sim}{\mathbf{E}}} = \frac{\partial \Delta \left(J \underset{\sim}{\sigma} \cdot \underset{\sim}{\mathbf{F}}^{-T} \right)}{\partial \Delta \underset{\sim}{\mathbf{E}}} = J(\mathbf{1} \underline{\otimes} \underset{\sim}{\mathbf{F}}^{-1}) : \frac{\partial \Delta \underset{\sim}{\sigma}}{\partial \Delta \underset{\sim}{\mathbf{E}}}, \tag{17.68}$$

$$\frac{\partial \underset{\sim}{\sigma}}{\partial \underset{\sim}{\mathbf{E}}} = -J_e^{-1}(\underset{\sim}{\mathbf{E}} \cdot \underset{\sim}{\Pi}^e \cdot \underset{\sim}{\mathbf{E}}^T) \otimes \underset{\sim}{\mathbf{E}}^{-T} + J_e^{-1} \mathbf{1} \underline{\otimes}(\underset{\sim}{\Pi}^e \cdot \underset{\sim}{\mathbf{E}}^T)^T$$

$$+ J_e^{-1}(\underset{\sim}{\mathbf{E}} \underline{\otimes} \mathbf{E}) : \frac{\partial \underset{\sim}{\Pi}^e}{\partial \underset{\sim}{\mathbf{E}}} + J_e^{-1} \left[(\underset{\sim}{\mathbf{E}} \cdot \Pi^e) \underline{\otimes} \mathbf{1} \right] : (\mathbf{1} \overline{\otimes} \mathbf{1}), \tag{17.69}$$

$$\frac{\partial \underset{\sim}{\Pi}^e}{\partial \underset{\sim}{\mathbf{E}}} = \frac{\partial \underset{\sim}{\Pi}^e}{\partial \underset{\sim}{\mathbf{E}}^e_{GL}} : \frac{\partial \underset{\sim}{\mathbf{E}}^e_{GL}}{\partial \underset{\sim}{\mathbf{E}}}, \tag{17.70}$$

$$\frac{\partial \underset{\sim}{\Pi}^e}{\partial \underset{\sim}{\mathbf{E}}^e_{GL}} = \underset{\sim}{\mathbf{C}}, \tag{17.71}$$

$$\frac{\partial \underset{\sim}{\mathbf{E}}^e_{GL}}{\partial \underset{\sim}{\mathbf{E}}} = \frac{1}{2}(\mathbf{1} \overline{\otimes} \mathbf{E}^T + \mathbf{E}^T \underline{\otimes} \mathbf{1}), \tag{17.72}$$

$$[L]_s = \frac{\partial R_{\text{in}}}{\partial \Delta v_{\text{IN}}} = \left(\frac{\dfrac{\partial R_{\underset{\sim}{\mathbf{E}}}}{\partial \Delta \underset{\sim}{\mathbf{F}}}}{[0]} \right), \tag{17.73}$$

$$\frac{\partial R_{\underset{\sim}{\mathbf{E}}}}{\partial \Delta \underset{\sim}{\mathbf{F}}} = -\mathbf{1} \underline{\otimes} \left(\mathbf{E}^T \cdot \underset{\sim}{\mathbf{F}}^{-T} \right) + (\Delta \underset{\sim}{\mathbf{F}} \underline{\otimes} \mathbf{E}^T) : (\underset{\sim}{\mathbf{F}}^{-1} \underline{\otimes} \underset{\sim}{\mathbf{F}}^{-T}). \tag{17.74}$$

17.4 Applications to a single-crystal turbine blade and a cylinder under torsion

The crystal elasto-plasticity model at finite strain presented in Section 17.3 is implemented in the finite element software Z-set [103,1]. The model is applied to predict the behavior of a single-crystal turbine blade and a single-crystal cylinder under torsion.

17.4.1 Single-crystal turbine blade

An interesting industrial application of the finite element implementation of crystal plasticity constitutive equations is, for instance, the computation of the behavior of a nickel-based superalloy single-crystal turbine blade. In service, such turbine blades are submitted to important centrifugal forces induced by the fast rotation ($\sim$ 20000 RPM) of the turbine disk they are attached to. In addition, during a single flight their operating temperature can vary over three orders of magnitude. For sake of sim-

TABLE 17.1 Numerical values of material parameters used for the simulation of a nickel-based superalloy single-crystal turbine blade.

C_{11} (GPa)	C_{12} (GPa)	C_{44} (GPa)	τ_0 (MPa)	n (—)	$\dot{\gamma}_0$ (s^{-1})	μ (GPa)	G_c (—)	κ (—)
204	125	112	235	15	200	65.6	10.4	42.8

r_0^s	a_1	a_2	a_3	a_4	a_5	a_6	$b_{s\neq u}^{su}$	b^{uu}
5.38e-5	0.124	0.124	0.07	0.625	0.137	0.122	1	0

plicity, we consider here a constant and uniform temperature and focus on the mechanical behavior of the blade as the rotation rate ω of the turbine linearly and indefinitely increases. Of course, such a loading history is unrealistic for nominal in-service conditions and is rather to be seen as a demonstration of the capabilities of the finite element model. Cubic elasticity moduli, critical resolved shear stress, and viscoplastic flow parameters identified at 650°C on the nickel-based superalloy DS200 by [293] are used. Octahedral slip systems families {110}⟨111⟩ are considered. Instead of the phenomenological kinematic hardening law used in [293] based on the work of [936], the dislocation-based isotropic hardening law presented in Section 17.2 is used. The material parameters are presented in Table 17.1. A fictional turbine blade geometry is meshed with 191147 linear tetrahedral elements reduced integrated with one Gauss point. The crystal is oriented such that the crystal directions triplet ([100] − [010] − [001]) coincide with the orthogonal basis vectors triplet $(\underline{X}_1, \underline{X}_2, \underline{X}_3)$.

The simulated von Mises equivalent stress field and cumulated plastic slip field are shown in Fig. 17.1 at an angular velocity $\omega = 30000$ RPM. To reach this velocity, a linear ramping was used with $\dot{\omega} = 31.9$ RPM/s. Highly loaded zones are located at notches present in the foot and at the junction between the foot and the body of the turbine blade as expected. Stress concentrations are also visible in the vicinity of cooling holes. Interestingly, the most plastically deformed region lies a little above the junction between the foot and the body of the turbine blade. This region concentrating most of plastic slip spreads across the whole cross-section orthogonal to the radial direction of the turbine $\underline{X}_3$. In particular, the highest levels of plastic deformations are located in the vicinity of cooling holes nearest to the turbine blade foot.

17.4.2 Single-crystal cylinder under torsion

The authors of [1026,457] investigated experimentally and numerically the behavior of single-crystal wires in torsion. They showed the existence of plastic slip gradients along the radius of wires, as well as along their circumference. The latter gradient is due to the anisotropic activation of slip systems. As already pointed out by [1026], the presence of circumferential strain gradients, visible in experiments, could not be predicted
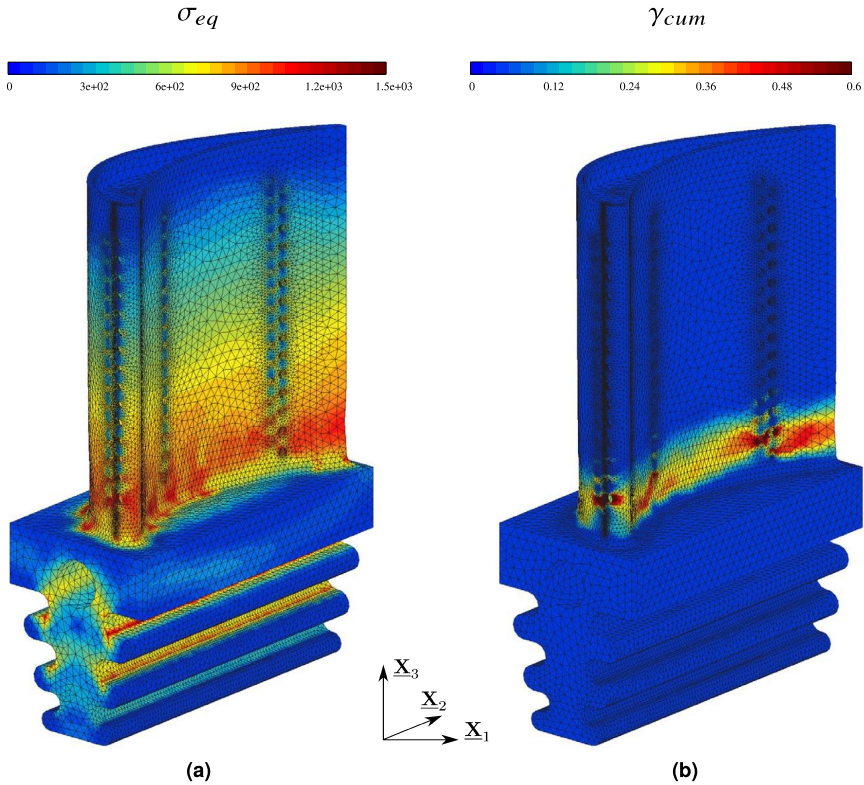
FIGURE 17.1 Simulated (a) von Mises stress and (b) cumulated plastic slip contours in a single crystal turbine blade.

by any quadratic yield criterion, such as, e.g., Hill's criterion. On the contrary, by computing analytically maximum Schmid factor maps, it appears clearly that Schmid's criterion predicts that some regions will yield earlier than others. As an example, octahedral slip systems families $\{110\}\langle111\rangle$ are considered. Four different orientations of the crystal in the cylinder are chosen such that the crystal directions triplets ($[100] - [010] - [001]$), ($[001] - [1\bar{1}0] - [110]$), ($[1\bar{1}0] - [11\bar{2}] - [111]$), and ($[12\bar{1}] - [\bar{2}10] - [125]$) respectively coincide with the orthogonal basis vectors triplet ($\underline{X}_1, \underline{X}_2, \underline{X}_3$). These crystal orientations are later denoted $\langle100\rangle$, $\langle110\rangle$, $\langle111\rangle$, and $\langle125\rangle$, respectively. The cylinder axis is aligned with $\underline{X}_3$. Fig. 17.2 displays the maximum Schmid factor maps in the cross-section of these cylinders. Sectors of maximum Schmid factor are indeed visible. Therefore, plastic slip will preferentially be activated in such zones and lead to circumferential plastic strain gradients. It should be noted that in a torsion test, the applied torsion stress $\tau_{\theta z}$ increases linearly with the radial position from the center

(a) $\langle 100 \rangle$ **(b)** $\langle 110 \rangle$ **(c)** $\langle 111 \rangle$ **(d)** $\langle 125 \rangle$
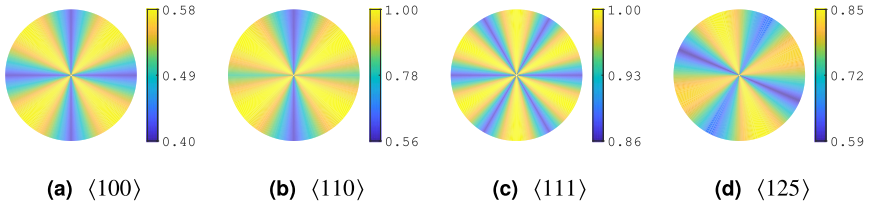
FIGURE 17.2 Maximum Schmid factor maps in the cross-section of single crystal cylinders with the middle axis respectively initially aligned with $\langle 100 \rangle$, $\langle 110 \rangle$, $\langle 111 \rangle$, and $\langle 125 \rangle$ crystal directions.

TABLE 17.2 Numerical values of material parameters for the simulation of stainless steel single crystal cylinders in torsion.

C_{11} (GPa)	C_{12} (GPa)	C_{44} (GPa)	τ_0 (MPa)	n (—)	$\dot{\gamma}_0$ (s^{-1})	μ GPa	G_c (—)	κ (—)
199	136	105	88	20	10^{29}	65.6	10.4	42.8

r_0^s	a_1	a_2	a_3	a_4	a_5	a_6	$b_{s \neq u}^{su}$	b^{uu}
5.38e-5	0.124	0.124	0.07	0.625	0.137	0.122	1	0

of the cylinder. As a consequence, a radial gradient of plastic activity is also to be expected.

The dislocation density based crystal plasticity model presented above is applied to pursue investigation of the behavior of single crystal cylinders under torsion. A single crystal cylinder of length L_0 and radius R_0 is put under torsion by prescribing nil displacements to its bottom face and a rotation rate to its upper face. In cylindrical coordinates, the displacement boundary conditions are written as

$$u_r(r, \theta, z = 0) = 0, \tag{17.75}$$

$$u_\theta(r, \theta, z = 0) = 0, \qquad u_\theta(r, \theta, z = L_0) = r\dot{\theta}, \tag{17.76}$$

$$u_z(r, \theta, z = 0) = 0. \tag{17.77}$$

The rotation rate $\dot{\theta}$ is taken as $2\pi \times 10^{-4}$ s^{-1}. Material parameters relevant for face-centered cubic (FCC) austenitic stainless steel single crystals with octahedral slips systems were used and are listed in Table 17.2. Cylinders are meshed with 12800 quadratic elements reduced integrated with 8 Gauss points.

The fields of cumulated plastic slip obtained with these four orientations are plotted in Fig. 17.3 on the outer surface in (a)–(d) and in the middle cross-section at $z = L_0/2$ in (e)–(h). The fields are plotted on the deformed mesh for a $\theta = 90°$ rotation of the top face with respect to the initial configuration. A characteristic patterning of plastic slip can indeed be observed. First of all, a radial gradient of plastic strain is obtained as expected. Additionally, plastic strains are also heterogeneous on the circumference of the single crystal cylinders because of the heterogeneity of

γ_{cum}
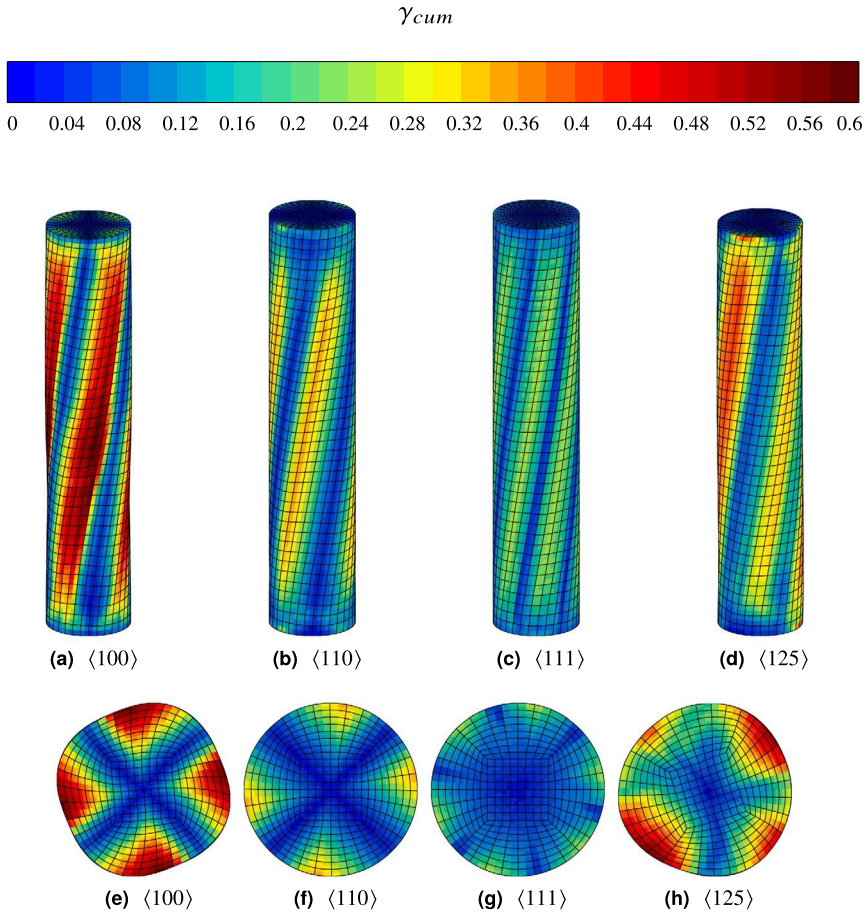
FIGURE 17.3 Simulated cumulated plastic slip contours on the outer surface (a)–(d) and in the middle cross-section (e)–(h) of single crystal cylinders at $\theta = 90°$, with the middle axis respectively initially aligned with $\langle 100 \rangle$, $\langle 110 \rangle$, $\langle 111 \rangle$, and $\langle 125 \rangle$ crystal directions and material parameters presented in Table 17.2.

the maximum Schmid factor depicted in Fig. 17.2. "Soft zones" concentrate most of plastic slip, while "hard zones" remain almost completely elastic. The number and intensity of such zones varies with the orientation of the crystal in the cylinder. For orientations $\langle 100 \rangle$ and $\langle 110 \rangle$, four "soft zones" of equal plastic intensity and four "hard zones" are clearly visible. For the $\langle 111 \rangle$ orientation, six zones of each kind and of equal intensities can be observed. The $\langle 125 \rangle$ orientation displays a more complex pattern. It is composed of two wide and intensely deformed "soft areas" and two additional "soft zones" which seem to be splitting in two narrower regions. Four "hard zones" are visible for this orientation.
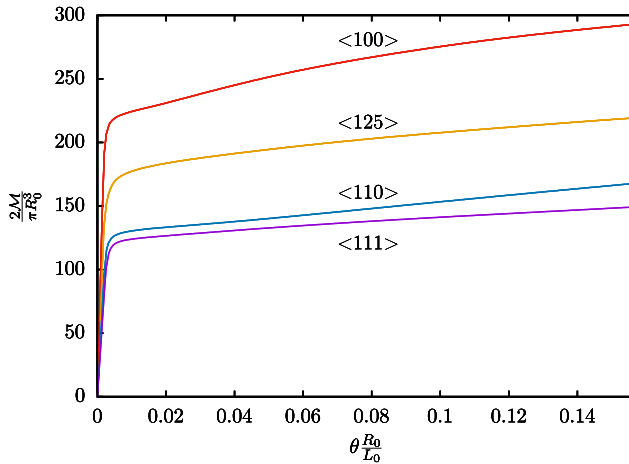
FIGURE 17.4 Simulated torque vs. shear strain curves for single crystal cylinders with the middle axis respectively initially aligned with ⟨100⟩, ⟨110⟩, ⟨111⟩, and ⟨125⟩ crystal directions and material parameters presented in Table 17.2.

In Fig. 17.4, we plotted the shear stress $2\mathcal{M}/\pi R_0^3$ against the shear strain $\theta R_0/L_0$, where $\mathcal{M}$ is the applied torque, for the four different crystal orientations. The hardest response is obtained with the ⟨100⟩ orientation, for which the maximum Schmid factor maps in Fig. 17.2 display the lowest maximum values ($\leq 1/\sqrt{3}$). The second hardest response corresponds to the ⟨125⟩ orientation for which it was shown in Fig. 17.2 that the maximum Schmid factor in the cross section does not exceed 0.85. Furthermore, ⟨110⟩ and ⟨111⟩ orientations display similar apparent yield stresses. These two orientations have indeed a maximum value of the maximum Schmid factors in the cylinder cross-section equal to 1. The ⟨111⟩ orientation appears to be a little softer than the ⟨110⟩ orientation because its average maximum Schmid factor value is the largest. Therefore the plastic slip field is the most heterogeneous for this orientation as seen in Fig. 17.3.

17.5 Extensions of constitutive equations: a reduced micromorphic model for single crystals

Conventional elasto-plasticity is known to be size-independent. Such an assumption is realistic when the size of the medium can be considered large with respect to the characteristic length of deformation mechanisms. However, it is hence unsuited in order to predict size effects arising at small scales. Nonlocal models that naturally introduce material length scales are therefore proficient extensions of conventional theories. They mainly resort on integral or gradient enhancements of conventional con-

stitutive equations. For example, among gradient-type formulations, the micromorphic approach [455] can be followed in order to extend the constitutive model for single crystals presented above. In this section, the finite element implementation of a reduced micromorphic single-crystal model at finite strains based on a scalar nonlocal variable is presented. Following [1588], a possible choice of nonlocal variable in the context of crystal plasticity is the cumulated plastic slip γ_{cum} defined as

$$\gamma_{cum} = \int_0^t \sum_{\alpha=1}^N |\dot{\gamma}^\alpha| \, dt. \tag{17.78}$$

Its micromorphic counterpart, denoted γ_χ, is called microslip. The latter is considered as an additional degree of freedom, on par with displacement degrees of freedom, as well as an input variable of the material behavior. Furthermore, the gradient of microslip $\underline{\mathbf{K}}_\chi = \text{Grad}\,\gamma_\chi$ is equally treated as an input variable. The generalized stresses, which are work conjugates of γ_χ and $\underline{\mathbf{K}}_\chi$, are respectively denoted by S and $\underline{\mathbf{M}}$. Just as the first Piola–Kirchhoff stress, they are output variables of the constitutive model. In addition to the conventional internal variables, the cumulated plastic slip γ_{cum} is treated as an additional variable to be integrated. To summarize, the following sets of input, output, and internal variables are considered:

$$v_{\text{IN}} : \{\underline{\mathbf{F}}, \gamma_\chi, \underline{\mathbf{K}}_\chi\}, \quad v_{\text{OUT}} : \{\underline{\mathit{\Pi}}, S, \underline{\mathbf{M}}\}, \quad v_{\text{in}} : \{\underline{\mathbf{E}}, \gamma^\alpha, r^\alpha, \gamma_{cum}\}. \tag{17.79}$$

The thermodynamical derivation of the present model is detailed in [844,1274]. It is based, first, on enrichment of the principle of virtual power to higher-order contributions [509]. From this generalization, one obtains a supplementary equilibrium equation and, for instance, Neumann boundary condition for any subdomain $\mathcal{D}$ of the material body

$$
\begin{aligned}
\text{Div}\,\underline{\mathbf{M}} - S &= 0 & \forall \underline{\mathbf{X}} \in \mathcal{D}, \\
M &= \underline{\mathbf{M}} \cdot \underline{\mathbf{n}}_0 & \forall \underline{\mathbf{X}} \in \partial D,
\end{aligned}
\tag{17.80}
$$

where M is a generalized traction scalar, power conjugate to $\dot{\gamma}_\chi$, and $\underline{\mathbf{n}}_0$ the outward normal unit vector in the initial configuration. Solving the weak form of Eq. (17.80), together with the conventional equilibrium equation and boundary condition ($\text{Div}\,(\underline{\mathit{\Pi}}) = 0$ and $\underline{\mathbf{T}} = \underline{\mathit{\Pi}} \cdot \underline{\mathbf{n}}_0$, in the absence of body forces), by finite elements can be done by following the procedure described in [844]. The second ingredient is a enhanced free energy potential ψ accounting for nonlocal contributions. Assuming a quadratic nonlocal potential, the conventional state law in Eq. (17.50) is complemented by two additional state laws for the generalized stresses S and

M,

$$\Delta S = -H_\chi(\Delta\gamma_{cum} - \Delta\gamma_\chi), \tag{17.81}$$

$$\Delta\underline{\mathbf{M}} = A\Delta\underline{\mathbf{K}}_\chi, \tag{17.82}$$

where H_χ and A are higher-order elasticity moduli; H_χ is a penalization parameter which usually takes large values in order to enforce quasiequality between γ_χ and γ_{cum}; A has the units of MPa·mm^2 and therefore bears the material characteristic length. The major outcome of the gradient-enhanced free energy potential is the modification of the residual mechanical dissipation, which now involves higher-order terms. It ensures an extension of the yield criteria in Eq. (17.20) and, equally, of the plastic flow rules in Eq. (17.21) as follows:

$$f_\chi^\alpha = |\tau^\alpha| - (\tau_c^\alpha - S) = |\tau^\alpha| - (\tau_c^\alpha + H_\chi(\gamma_{cum} - \gamma_\chi)), \tag{17.83}$$

$$\Delta\gamma^\alpha = \text{sign}\left(\tau^\alpha\right)\Delta t\,\dot{\gamma}_0\Phi(f_\chi^\alpha), \qquad \Phi(f_\chi^\alpha) = \left\langle\frac{f_\chi^\alpha}{\tau_0^\alpha}\right\rangle^n. \tag{17.84}$$

The generalized scalar stress S, depending on its sign, acts locally as an additional hardening or softening contribution. By combining Eqs. (17.80) and (17.82), we obtain $S = \text{Div}(A\text{Grad}\,\gamma_\chi)$. Therefore, locally, a positive curvature of γ_χ induces softening; conversely, a locally negative curvature of γ_χ introduces additional hardening. Increments of cumulated plastic slip must satisfy Eq. (17.78), which gives

$$\Delta\gamma_{cum} = \sum_{\alpha=1}^{N}|\Delta\gamma^\alpha|. \tag{17.85}$$

The set of residual equations for the reduced micromorphic single-crystal model at finite strains become

$$R_{\text{in}} = \begin{cases} R_{\underline{E}} = \Delta\underline{\mathbf{E}} - \Delta\underline{\mathbf{F}}\cdot\underline{\mathbf{F}}^{-1}\cdot E - \underline{\mathbf{E}}\cdot\left(\sum_{\alpha=1}^{N}\Delta\gamma^\alpha\mathbf{N}^\alpha\right), \\[2mm] R_{\gamma^\alpha} = \Delta\gamma^\alpha - \text{sign}\left(\tau^\alpha\right)\Delta t\,\dot{\gamma}_0\Phi(f_\chi^\alpha), \\[2mm] R_{r^\alpha} = \Delta r^\alpha - |\Delta\gamma^\alpha|\left(\frac{1}{\kappa}\sqrt{\sum_{\beta=1}^{N}b^{\alpha\beta}r^\beta} - G_c r^\alpha\right), \\[2mm] R_{\gamma_{cum}} = \Delta\gamma_{cum} - \sum_{\alpha=1}^{N}|\Delta\gamma^\alpha|. \end{cases} \tag{17.86}$$

It is remarkable how corresponding residuals in Eq. (17.86) are similar to their conventional counterparts; $R_{\underline{E}}$ and R_{r^α} are indeed completely un-

changed, while R_{γ^α} is only slightly modified, and the straightforward term $R_{\gamma_{cum}}$ is added. The Jacobian matrix $[J]$ can accordingly be computed without much difficulty, since only the last row and column need to be given, while other terms remain formally unchanged given that f^α is replaced by f_χ^α:

$$
[J] = \frac{\partial R_{\text{in}}}{\partial \Delta v_{\text{int}}} = \begin{pmatrix} \dfrac{\partial R_{\underset{\sim}{E}}}{\partial \Delta \underset{\sim}{\mathbf{E}}} & \dfrac{\partial R_{\underset{\sim}{E}}}{\partial \Delta \gamma^\beta} & \dfrac{\partial R_{\underset{\sim}{E}}}{\partial \Delta r^\beta} & \dfrac{\partial R_{\underset{\sim}{E}}}{\partial \Delta \gamma_{cum}} \\[2.2ex] \dfrac{\partial R_{\gamma^\alpha}}{\partial \Delta \underset{\sim}{\mathbf{E}}} & \dfrac{\partial R_{\gamma^\alpha}}{\partial \Delta \gamma^\beta} & \dfrac{\partial R_{\gamma^\alpha}}{\partial \Delta r^\beta} & \dfrac{\partial R_{\gamma^\alpha}}{\partial \Delta \gamma_{cum}} \\[2.2ex] \dfrac{\partial R_{r^\alpha}}{\partial \Delta \underset{\sim}{\mathbf{E}}} & \dfrac{\partial R_{r^\alpha}}{\partial \Delta \gamma^\beta} & \dfrac{\partial R_{r^\alpha}}{\partial \Delta r^\beta} & \dfrac{\partial R_{r^\alpha}}{\partial \Delta \gamma_{cum}} \\[2.2ex] \hline \dfrac{\partial R_{\gamma_{cum}}}{\partial \Delta \underset{\sim}{\mathbf{E}}} & \dfrac{\partial R_{\gamma_{cum}}}{\partial \Delta \gamma^\beta} & \dfrac{\partial R_{\gamma_{cum}}}{\partial \Delta r^\beta} & \dfrac{\partial R_{\gamma_{cum}}}{\partial \Delta \gamma_{cum}} \end{pmatrix} . \qquad (17.87)
$$

After straightforward derivations, one obtains

$$
\frac{\partial R_{\underset{\sim}{E}}}{\partial \Delta \gamma_{cum}} = 0, \tag{17.88}
$$

$$
\frac{\partial R_{\gamma^\alpha}}{\partial \Delta \gamma_{cum}} = -\text{sign}\left(\tau^\alpha\right) \Delta t \frac{\partial \Phi^\alpha}{\partial f_\chi^\alpha} \frac{\partial f_\chi^\alpha}{\partial \gamma_{cum}} = \text{sign}\left(\tau^\alpha\right) \frac{\Delta t \dot{\gamma}_0 n}{(\tau_0^\alpha)^n} \left\langle \frac{f_\chi^\alpha}{\tau_0^\alpha} \right\rangle^{n-1} H_\chi, \tag{17.89}
$$

$$
\frac{\partial R_{r^\alpha}}{\partial \Delta \gamma_{cum}} = 0, \tag{17.90}
$$

$$
\frac{\partial R_{\gamma_{cum}}}{\partial \Delta \underset{\sim}{\mathbf{E}}} = 0, \tag{17.91}
$$

$$
\frac{\partial R_{\gamma_{cum}}}{\partial \Delta \gamma^\beta} = -\text{sign}\left(\Delta \gamma^\beta\right), \tag{17.92}
$$

$$
\frac{\partial R_{\gamma_{cum}}}{\partial \Delta r^\beta} = 0, \tag{17.93}
$$

$$
\frac{\partial R_{\gamma_{cum}}}{\partial \Delta \gamma_{cum}} = 1. \tag{17.94}
$$

Since additional input and output variables are considered, the consistent tangent operator incorporates the following additional derivatives:

- $\dfrac{\partial \Delta v_{\mathrm{OUT}}}{\partial \Delta v_{\mathrm{IN}}}$

$$\frac{\partial \Delta \underset{\sim}{\Pi}}{\partial \Delta \mathbf{F}} = \text{see Eq. (17.66)}, \quad \frac{\partial \Delta \underset{\sim}{\Pi}}{\partial \Delta \gamma_\chi} = 0, \quad \frac{\partial \Delta \underset{\sim}{\Pi}}{\partial \Delta \underline{\mathbf{K}}_\chi} = 0,$$

$$\frac{\partial \Delta S}{\partial \Delta \mathbf{F}} = 0, \quad \frac{\partial \Delta S}{\partial \Delta \gamma_\chi} = H_\chi, \quad \frac{\partial \Delta S}{\partial \Delta \underline{\mathbf{K}}_\chi} = 0, \qquad (17.95)$$

$$\frac{\partial \Delta \underline{\mathbf{M}}}{\partial \Delta \mathbf{F}} = 0, \quad \frac{\partial \Delta \underline{\mathbf{M}}}{\partial \Delta \gamma_\chi} = 0, \quad \frac{\partial \Delta \underline{\mathbf{M}}}{\partial \Delta \underline{\mathbf{K}}_\chi} = A;$$

- $\dfrac{\partial \Delta v_{\mathrm{OUT}}}{\partial \Delta v_{\mathrm{in}}}$

$$\frac{\partial \Delta \underset{\sim}{\Pi}}{\partial \Delta \underset{\sim}{\mathbf{E}}} = \text{see Eq. (17.68)}, \quad \frac{\partial \Delta \underset{\sim}{\Pi}}{\partial \Delta \gamma^\beta} = 0, \quad \frac{\partial \Delta \underset{\sim}{\Pi}}{\partial \Delta r^\beta} = 0, \quad \frac{\partial \Delta \underset{\sim}{\Pi}}{\partial \Delta \gamma_{cum}} = 0,$$

$$\frac{\partial \Delta S}{\partial \Delta \underset{\sim}{\mathbf{E}}} = 0, \quad \frac{\partial \Delta S}{\partial \Delta \gamma^\beta} = 0, \quad \frac{\partial \Delta S}{\partial \Delta r^\beta} = 0, \quad \frac{\partial \Delta S}{\partial \Delta \gamma_{cum}} = -H_\chi,$$

$$\frac{\partial \Delta \underline{\mathbf{M}}}{\partial \Delta \underset{\sim}{\mathbf{E}}} = 0, \quad \frac{\partial \Delta \underline{\mathbf{M}}}{\partial \Delta \gamma^\beta} = 0, \quad \frac{\partial \Delta \underline{\mathbf{M}}}{\partial \Delta r^\beta} = 0, \quad \frac{\partial \Delta \underline{\mathbf{M}}}{\partial \Delta \gamma_{cum}} = 0;$$

$$(17.96)$$

- $[L]_s = \dfrac{\partial R_{\mathrm{in}}}{\partial \Delta v_{\mathrm{IN}}}$

$$\frac{\partial R_{\underset{\sim}{E}}}{\partial \Delta \mathbf{F}} = \text{see Eq. (17.74)}, \quad \frac{\partial R_{\underset{\sim}{E}}}{\partial \Delta \gamma_\chi} = 0, \quad \frac{\partial R_{\underset{\sim}{E}}}{\partial \Delta \underline{\mathbf{K}}_\chi} = 0,$$

$$\frac{\partial R_{\gamma^\alpha}}{\partial \Delta \mathbf{F}} = 0, \quad \frac{\partial R_{\gamma^\alpha}}{\partial \Delta \gamma_\chi} = -\text{sign}\left(\tau^\alpha\right) \frac{\Delta t \dot{\gamma}_0 n}{(\tau_0^\alpha)^n} H_\chi, \quad \frac{\partial R_{\gamma^\alpha}}{\partial \Delta \underline{\mathbf{K}}_\chi} = 0,$$

$$\frac{\partial R_{r^\alpha}}{\partial \Delta \mathbf{F}} = 0, \quad \frac{\partial R_{r^\alpha}}{\partial \Delta \gamma_\chi} = 0, \quad \frac{\partial R_{r^\alpha}}{\partial \Delta \underline{\mathbf{K}}_\chi} = 0,$$

$$\frac{\partial R_{\gamma_{cum}}}{\partial \Delta \mathbf{F}} = 0, \quad \frac{\partial R_{\gamma_{cum}}}{\partial \Delta \gamma_\chi} = 0, \quad \frac{\partial R_{\gamma_{cum}}}{\partial \Delta \underline{\mathbf{K}}_\chi} = 0.$$

$$(17.97)$$